Biomechanical properties of murine meniscus surface via AFM-based nanoindentation

Citation: Li, Qing et al. "Biomechanical Properties of Murine Meniscus Surface via AFM-Based Nanoindentation." Journal of Biomechanics 48.8 (2015): 1364–1370.

As Published: http://dx.doi.org/10.1016/j.jbiomech.2015.02.064

Publisher: Elsevier

Persistent URL: http://hdl.handle.net/1721.1/106567

Version: Author's final manuscript: final author's manuscript post peer review, without publisher's formatting or copy editing

HHS Public Access

Author manuscript

J Biomech. Author manuscript; available in PMC 2016 June 01.

Published in final edited form as:

J Biomech. 2015 June 1; 48(8): 1364–1370. doi:10.1016/j.jbiomech.2015.02.064.

Biomechanical Properties of Murine Meniscus Surface via AFM-based Nanoindentation

Qing Li[1], **Basak Doyran**[1], **Laura W. Gamer**[2], **X. Lucas Lu**[3], **Ling Qin**[4], **Christine Ortiz**[5], **Alan J. Grodzinsky**[6,7,8], **Vicki Rosen**[2], and **Lin Han**[1,*]

[1]School of Biomedical Engineering, Science, and Health Systems, Drexel University, Philadelphia, PA 19104, United States

[2]Department of Developmental Biology, Harvard School of Dental Medicine, Boston, MA 02115, United States

[3]Department of Mechanical Engineering, University of Delaware, Newark, DE 19716, United States

[4]Department of Orthopaedic Surgery, University of Pennsylvania, Philadelphia, PA 19104, United States.

[5]Department of Materials Science and Engineering, Massachusetts Institute of Technology, Cambridge, MA 02139, United States

[6]Department of Biological Engineering, Massachusetts Institute of Technology, Cambridge, MA 02139, United States

[7]Department of Electrical Engineering and Computer Science, Massachusetts Institute of Technology, Cambridge, MA 02139, United States

[8]Mechanical Engineering Massachusetts Institute of Technology, Cambridge, MA 02139, United States

Abstract

This study aimed to quantify the biomechanical properties of murine meniscus surface. Atomic force microscopy (AFM)-based nanoindentation was performed on the central region, proximal side of menisci from 6- to 24-week old male C57BL/6 mice using microspherical tips ($R_{tip} \approx 5$ μm) in PBS. A unique, linear correlation between indentation depth, D, and response force, F, was found on menisci from all age groups. This non-Hertzian behavior is likely due to the dominance of tensile resistance by the collagen fibril bundles on meniscus surface that are mostly aligned

*Correspondence and requests for materials should be addressed to: Dr. Lin Han Phone: (215)571-3821 Fax: (215)895-4983 lh535@drexel.edu..

Conflict of interest statement

The authors of this study have no personal or financial conflicts of interest with this work. All authors were fully involved in the study and preparation of this manuscript and the material within has not been and will not be submitted for publication elsewhere.

along the circumferential direction observed on 12-week old menisci. The indentation resistance was calculated as both the effective stiffness, $S_{ind} = dF/dD$, and the effective modulus, E_{ind}, via the isotropic Hertz model. Values of S_{ind} and E_{ind} were found to depend on indentation rate, suggesting the existence of poro-viscoelasticity. These values do not significantly vary with anatomical sites, lateral versus medial compartments, or mouse age. In addition, E_{ind} of meniscus surface (e.g., 6.1 ± 0.8 MPa for 12 weeks of age, mean ± SEM, n = 13) was found to be significantly higher than those of meniscus surfaces in other species, and of murine articular cartilage surface (1.4 ± 0.1 MPa, n = 6). In summary, these results provided the first direct mechanical knowledge of murine knee meniscus tissues. We expect this understanding to serve as a mechanics-based benchmark for further probing the developmental biology and osteoarthritis symptoms of meniscus in various murine models.

Keywords

meniscus; mouse models; atomic force microscopy; nanoindentation; anisotropy

1. Introduction

Knee meniscus is a hydrated fibrocartilage tissue with an extracellular matrix (ECM) mainly composed of circumferentially aligned, type I-dominated collagen fibers (≈ 20 – 25 wet wt %) and small amounts of proteoglycans (< 5 wet wt%) (Aspden et al., 1985; Herwig et al., 1984). In human menisci, the circumferential fibers are wrapped within the superficial layer made of radially aligned fibers, which is covered by a thin mesh of transversely aligned fibrils on the surface (Petersen and Tillmann, 1998). Within the interior of the meniscus, circumferential fibers are further interdigitated by “radial-tie” fibers throughout (Skaggs et al., 1994). This hierarchically structured, heterogeneous ECM provides meniscus with its biomechanical functions paramount to joint motion, including load distribution (Walker and Erkman, 1975), shock absorption (Voloshin and Wosk, 1983) and lubrication (Fithian et al., 1990). During the progression of osteoarthritis (OA), meniscus often undergoes maceration, tear or even total damage that leads to the loss of its biomechanical functions (Katsuragawa et al., 2010). These symptoms contribute to the abnormal joint loading, and further accelerate the degeneration of cartilage (Englund, 2008; Hunter et al., 2006; Klompmaker et al., 1992). Knowledge about the structure-mechanics relationships of meniscus ECM is thus critical for understanding joint function, documenting disease progression and designing repair strategies (Makris et al., 2011).

In the past decades, the mechanical properties of menisci in human and animals have been extensively explored via both experimental (Baro et al., 2012; Fithian et al., 1990; Proctor et al., 1989; Sweigart and Athanasiou, 2005) and theoretical (Spilker et al., 1992) approaches. These studies have established a knowledge base of meniscus biomechanics across species. However, biomechanical knowledge of meniscus in one critical species, mouse, is lacking. Murine models offer a unique platform to study synovial joint development and OA pathology due to its short lifespan, low cost of maintenance and availability for genetic modification (Ameye and Young, 2006; Fang and Beier, 2014). Limited by its relatively small tissue size, conventional mechanical tests are not applicable to evaluate the structure

or mechanical properties of murine menisci. Without this understanding, it is challenging to study joint development or OA degradation in murine models from the perspective of meniscus biomechanics.

The objective of this study was to define the biomechanical properties of murine meniscus surface. Using atomic force microscopy (AFM)-based nanoindentation, we quantified the indentation responses of the meniscus surface from normal, male C57BL/6 mice. This study revealed the impacts of indentation rate, anatomical location and age on the mechanical properties. The indentation responses were interpreted in the context of meniscus surface collagen fibril structure quantified on 12-week old tissues. Results were compared with menisci from other species, as well as murine articular cartilage to highlight the unique properties of murine meniscus. We expect the knowledge learned from the evaluation of healthy murine meniscus to serve as a benchmark for future investigations of OA-associated mechanical symptoms of meniscus surface in various transgenic or surgery-induced murine models.

2. Methods

2.1 Sample preparation

Hind knee menisci were harvested from male C57BL/6 mice at 6, 8, 12 and 24 weeks of ages (The Jackson Laboratory, Bar Harbor, ME) via release from the meniscus-tibial tendons. Freshly dissected samples were maintained in phosphate buffered saline (PBS, pH = 7.4) with protease inhibitors (Pierce Protease Inhibitor Tablets #88266, Thermo Fisher Scientific, Rockford, IL) at 4°C for less than 24 hours prior to mechanical tests. For each mouse, we tested the proximal side of both lateral and medial menisci. For the same mouse, we did not observe statistical differences in the mechanical properties of tissues from left versus right legs. We therefore tested either left or right knee menisci from one mouse, or pooled the data on the menisci of the same mouse.

Histology images were taken to show the overall morphology and location of ossification. Right knee joints from each of the 8- and 24-week old mice were harvested, decalcified, and embedded in paraffin. Serial 5-μm-thick sagittal sections were cut across the joint medial compartment. Safranin-O/FastGreen staining images showed that ossification at the anterior and posterior horns increased with age, with larger ossicles at the anterior end (Fig. 1a). This observation was consistent with previous studies (Pedersen, 1949). However, the ~ 50 – 100 μm thick central region for nanoindentation test was not ossified up to 24 weeks of age.

2.2 Atomic force microscopy (AFM)-based nanoindentation

Each meniscus was mounted on a stainless steel AFM disk via cyanoacrylate glue (Pelco Pro C300, Ted Pella, Inc.). Care was taken to ensure that the glue did not cover or infiltrate through the < 1 mm thick meniscus tissue, as later on confirmed by scanning electron microscope (SEM) images. For each meniscus, AFM-based nanoindentation was performed on the surface of the central, non-ossified region using a microspherical probe tip and a Dimension Icon AFM (BrukerNano, Santa Barbra, CA) (Fig. 1b). The spherical tip was prepared by attaching a borosilicate colloid (R_{tip} = 5.3 ± 0.4 μm, mean ± STD on n = 120

colloids measured via optical microscope, Polysciences, Warrington, PA) onto the tipless cantilever (nominal spring constant $k \approx 7.4$ N/m, AIO-TL tip C, NanoAndMore, Lady's Island, SC) using the M-Bond 610 epoxy (Polysciences) under the Dimension Icon AFM. For each meniscus, at least 10 different locations were tested up to an indentation depth of ≈ 0.3 μm at 10 μm/s rates. In addition, to study the rate-dependent mechanical properties of murine meniscus, for 8-week old murine menisci, indentation was repeated at 0.316 – 10 μm/s rates at each location. Each nanoindentation was found to result in negligible irreversible plastic deformation of the tissue, as suggested by the high repeatability of indentation curves at the same location and same indentation rate. Furthermore, to directly compare to the mechanical properties of murine articular cartilage, nanoindentation was also performed on the right hind knee medial condyle articular cartilage of 12-week old male mice at 10 μm/s indentation depth rate, following previously established procedures (Batista et al., 2014). During all the indentation measurements, meniscus and cartilage tissues were immersed in 0.15 M PBS (pH = 7.4) with protease inhibitors (Pierce) to maintain the physiological-like fluid environment.

2.3 Indentation data analysis

Each indentation force versus depth, *F-D*, curve was analyzed by two methods (Fig. 1c). First, following our previous established procedure on articular cartilage (Han et al., 2011), we calculated the effective indentation modulus, E_{ind}, at each rate by fitting the entire portion of each loading *F-D* curve with Hertz model via least squares linear regression (LSLR),

$$F=\frac{4}{3}\frac{E_{ind}}{(1-\nu^2)}R_{tip}^{1/2}D^{3/2}, \quad (1)$$

where R_{tip} is the tip radius (≈ 5 μm), and [g542] is the Poisson's ratio (≈ 0 for meniscus). The choice of Poisson's ratio was based on the estimate from tissue-level studies on other species (Sweigart et al., 2004). However, varying [g542] from 0 – 0.5 only yielded ≈ 25% difference in calculated E_{ind}, and did not affect the conclusions of this study.

Secondly, for each *F-D* curve, we calculated the effective indentation stiffness, S_{ind}, as the slope of the entire portion of the loading curve via LSLR,

$$S_{ind}=\frac{dF}{dD}, \quad (2)$$

The coefficient of determination, R^2, was used to compare the goodness-of-fit by these two methods. For all the *F-D* curves, the tip-sample adhesion forces were found to be negligible compared to the indentation forces (~ 1 μN, Fig. 1c).

2.4 Scanning electron microscopy (SEM) and tapping mode AFM imaging

To qualitatively interpret the biomechanical properties of murine meniscus in the context of its matrix collagen structure, serial enzymatic digestions were carried out to enable direct visualization of collagen fibril structure on the surface of 12-week old murine menisci. Immediately after nanoindentation, menisci were incubated in 0.1 mg/mL bovine pancreatic

trypsin (Sigma-Aldrich, St. Louis, MO) in PBS (pH = 7.4) at 37 °C for 24 h to remove proteoglycans, as previously described (Rojas et al., 2014). Tissues were then incubated in 0.4 U/mL hyaluronidase (Sigma-Aldrich) in PBS with 10mM sodium acetate (pH = 6.0) at 37 °C for 24 h to remove hyaluronan (Vanden Berg-Foels et al., 2012). After the digestion, samples were fixed with Karnovsky's fixative (Electron Microscopy Sciences, Hatfield, PA) for 3 h at room temperature, and then rinsed thoroughly with deionized water to remove chemical residuals. The samples were first dehydrated in a series of graded ethanol-water mixtures (ethanol volume ratio: 25%, 50%, 75%, 80% and 100%), each for two 10 min immersions. They were then immersed in a series of graded mixtures of hexamethyldisilazane (HMDS) (Sigma-Aldrich) and ethanol (HMDS volume ratio: 25%, 50%, 75% and 100%), each for two 10 min immersions (Bray et al., 1993). As surface tension was minimized in HMDS, the samples were dried in air overnight to retain the 3D architecture of the collagen structure and stored in a desiccator prior to imaging.

For tapping mode AFM imaging, a nanosized, pyramidal AFM tip (nominal $R_{tip} \approx 10$ nm, nominal $k \approx 42$ N/m, NCHV, BrukerNano) was used to visualize the meniscus surface collagen fibril architecture ($n = 3$ medial menisci at 12 weeks of age) in ambient conditions using the Dimension Icon AFM. For SEM imaging, additional samples ($n = 3$ medial menisci at 12 weeks of age) were thermally coated with 10 nm platinum, and imaged immediately via SEM (Supra 50vp, Zeiss, Peabody, MA). For both SEM and AFM images, the distributions of collagen diameter and alignment angle, [g537], with respect to the circumferential direction were manually measured via ImageJ.

2.5 Statistical analysis

Non-parametric statistical tests were used to avoid the assumption of normal distribution. Mann-Whitney U test was performed on the average S_{ind}, or E_{ind}, of menisci from each mouse to detect whether S_{ind} or E_{ind} vary significantly between the lateral versus medial compartments, or vary between meniscus and cartilage. Kruskal-Wallis test was performed to detect the variations with respect to indentation regions (inner, middle and outer), and mouse age. Friedman test was performed to examine the rate dependence of E_{ind} or S_{ind}. To compare the linear fit versus Hertz model, Wilcoxon signed-rank test was performed on the average coefficient of determination, R^2, obtained on each mouse with both fits. Except for those presented in Fig. 2b, data obtained on one mouse were pooled, as no significant differences were found between left versus right meniscus, or between medial versus lateral compartments. In all the tests, a p-value of less than 0.05 was taken as statistically significant.

3. Results

For all menisci, most indents yielded a unique, non-Hertzian indentation response. The *F-D* curves were found to behave more linearly at all tested rates, rather than the typical $F \sim D^{3/2}$ Hertzian pattern (Fig. 1c). For each *F-D* curve, S_{ind} was calculated to provide a more precise description of the *F-D* dependence. The Hertz model-based E_{ind} was also calculated to enable direct comparison with the moduli of menisci in other species, and to those of murine articular cartilage.

We did not find significant heterogeneity across different anatomical locations. On the proximal side of each meniscus, S_{ind} was found not to vary significantly across the inner, middle and outer regions (Fig. 2a). We therefore pooled the data obtained at all three regions from each meniscus. In addition, absence of significance in S_{ind} was found between the lateral and medial menisci (Fig. 2b). Similar to other soft tissues, significant rate dependence was detected here, where increasing indentation rate from 0.316 to 10 μm/s significantly increased S_{ind}. Furthermore, the linear *F-D* behaviors were persistent at all the tested rates (Fig. 3).

Within the tested murine age from 6 to 24 weeks, we did not find significant trend in S_{ind} (or E_{ind}). S_{ind} was found to be 9.6 ± 1.0 N/m, 7.8 ± 1.0 N/m, 7.3 ± 0.9 N/m and 7.5 ± 1.0 N/m at 6, 8, 12 and 24 weeks of age, respectively (Fig. 4a). When the Hertz model was applied, E_{ind} was 9.2 ± 1.6 MPa, 6.7 ± 1.1 MPa, 6.1 ± 0.8 MPa and 7.0 ± 1.2 MPa, at 6, 8, 12 and 24 weeks of age, respectively (Fig. 4b). In all tested ages, the coefficient of determination in LSLR, R^2, was significantly higher when using the linear fit than using the Hertz model (Fig. 4c). When compared to its direct contact counterpart, the articular cartilage surface, the murine meniscus surface appeared much stiffer. As shown in Fig. 5, nanoindentation on 12-week old murine cartilage yielded E_{ind} of 1.4 ± 0.1 MPa, ≈ 4 × lower than the moduli of meniscus at the same age.

Results from tapping mode AFM and SEM imaging on 12-week old meniscus surfaces were consistent ($p > 0.05$ via Mann-Whitney test), and were therefore pooled for analysis. The images yielded unique structural features of murine meniscus surface. Unlike the human tissues, we found the majority of surface collagen fibrils are aligned nearly along the circumferential direction as fibril bundles (Fig. 6a-c). The diameters of collagen fibrils were found to be 49.8 ± 9.5 nm (mean ± STD of 325 fibrils on the medial menisci of six 12-week old mice, 232 from SEM and 93 from AFM, Fig. 6d), similar to those of C57BL6 wild-type murine articular cartilage surface (Batista et al., 2014). In addition, the absolute values of the angle of each fibril alignment with respect to the circumferential direction, [g537], were found to be 21.9 ± 20.7° (429 fibrils on six 12-week old mice, 324 from SEM and 105 from AFM, Fig. 6e). The median of [g537] was 15.0°. As shown by the distribution of [g537], in addition the dominance of circumferentially aligned fibril bundles, there also existed transversely aligned fibrils interdigitating throughout these circumferential fibril bundles (e.g., white arrowheads in Fig. 6b,c), with a marginal preferential alignment along the radial direction (e.g., 3.7% of fibrils at 70° fl [g537] < 80°, Fig. 6e).

4. Discussion

4.1 Non-Hertzian indentation responses of murine meniscus surface

The linear *F-D* indentation response of murine meniscus surface is reported here for the first time (Figs. 1c, 3 and 5). This non-Hertzian behavior likely originates from the densely packed, highly anisotropic collagen fibril structure of the meniscus surface (Fig. 6). As revealed by SEM and AFM imaging on the 12-week old menisci, the surface is dominated by densely packed, circumferentially aligned fibril bundles, interdigitated by sparsely distributed, transversely aligned fibrils (white arrowheads in Fig. 6b,c). This structure leads to substantial tension-compression asymmetry. When nanoindentation was performed

normal to the surface, forces could mainly originate from the fibril tension resistance. In such highly aligned, densely packed fibril bundles, when fibril stretching, rather than uncrimping/realignment, dominates its deformation, stresses can travel along the fibrils much further beyond the local contact region (Wang et al., 2014). In this experiment, stresses likely transmit along the fibril bundles to a distance orders of magnitude (>> 10 μm) greater than the tip-sample contact radius (≈ 2.2 μm at 0.5 μm indentation depth). As a result, stresses were not localized, and indentation forces may not directly scale with the tip-sample contact area, as would be predicted by the Hertz model.

Another possible origin of this non-Hertzian response is the time-dependent poroviscoelasticity. It has been shown that when the indentation time is comparable with the characteristic viscoelasticity time (t_{indent}/[g306]$_{visco}$ ~ 1), *F-D* curves measured by a spherical tip follows a linear pattern (Sakai, 2002). However, we observed the linear *F-D* curves at all indentation rates (0.316 – 10 μm/s, Fig. 3a), rather than at one particular rate. While the rate dependent indentation behavior was only reported for 8-week old menisci (Fig. 3), this linear *F-D* relationship was found to persist at other ages (6 – 24 weeks) in the range of 0.1 – 10 μm/s indentation rates as well (*data not shown*). Thus, it is less likely that poroviscoelasticity is the dominating factor. We hypothesize that the tension resistance of meniscus surface collagen fibrils is the main factor of this non-Hertzian *F-D* response, while poroviscoelastic time-dependence may play a minor role. Current studies are aimed at quantitatively investigating the origins of this non-Hertzian response by combining AFM imaging, AFM-nanoindentation at different length scales and fibril-reinforce finite element models (Soulhat et al., 1999) to quantitatively reveal the nanostructure-nanomechanics relationships of murine meniscus and the associated age-dependence.

4.2 Absence of anatomical location dependence

We did not observe significant variations in S_{ind} (or E_{ind}) across the inner to outer regions on each meniscus (Fig. 2a), or between the lateral versus medial menisci (Fig. 2b). This lack of mechanical heterogeneity may be associated with the unique biomechanical functions of the meniscus surface. These functions include load distribution and transmission with cartilage, and the maintenance of meniscus tissue structural integrity (Andriacchi et al., 2004; Walker and Erkman, 1975). A structurally more homogeneous surface layer could be more effective in distributing stress to the interior and may reduce the risk of meniscus tear. This phenomenon of homogeneity is consistent with previous studies on the instantaneous modulus of skeletally mature porcine meniscus measured by AFM-nanoindentation (Sanchez-Adams et al., 2013), and local tissue strain distribution of young bovine menisci via depth-dependent strain monitoring (Lai and Levenston, 2010). Interestingly, this relative homogeneity of the surface is in high contrast to the salient heterogeneity of the interior meniscus. Different regions in the meniscus interior are known to have distinctive mechanical functions. As shown previously for porcine menisci, the outer (red) zone that mainly sustains circumferential tensile stresses is mechanically distinct from the inner (white) zone (Sanchez-Adams et al., 2013) that mostly undergoes compression (Makris et al., 2011).

4.3 Absence of age-dependence

We also did not observe significant age-dependence in S_{ind} or E_{ind} from young, immature (6 weeks) to mature (24 weeks) mice (Fig. 4). This lack of age-dependence could be attributed to the dominance of type I collagen-based fibrils and negligible concentration of proteoglycan content on meniscus surface (Moyer et al., 2013), as the turnover of collagen is known to be markedly longer than other matrix constituents. For example, in human femoral head cartilage, the metabolic half-life of type II-dominated collagen is ≈ 117 years (Verzijl et al., 2000), while that of aggrecan is ≈ 3.4 years (Maroudas et al., 1998). In human skin, the half-life of type I-dominated collagen is ≈ 15 years (Verzijl et al., 2000). The half-life of murine meniscus collagen has not been quantified. However, it is reasonable to expect a collagen network half-life comparable to the life expectancy of mice, or at least, to the age span (6 to 24 weeks) of this study. It is therefore likely that meniscus structure and mechanics exhibit much less age-dependent variations within the tested age than the aggrecan-rich cartilage. Interestingly, while we did not find significant age dependence in meniscus (Fig. 4), the density and modulus of cortical bone from the same C57BL/6 mouse strain was found to significantly increase with age within 4 to 24 weeks of age. However, this increase in modulus was marginal after 8 weeks of age, and was highly correlated with increase in the degree of mineralization (Somerville et al., 2004). For the central region of meniscus, in the absence of mineralization, the temporal trend of development and maturation could be different from that of cortical bone. We believe that future studies targeted to younger and older mice can further elucidate the mechanical implications of the meniscus and its association with skeletal development and aging.

4.4 Comparison to meniscus of other species

Interestingly, the murine meniscus surface showed significantly higher E_{ind} than those of other species measured via nano- to microindentations. In this study, E_{ind} for 12-week old menisci was 6.1 ± 0.8 MPa (Fig. 3b). In comparison, for skeletally mature porcine meniscus surface, AFM-based nanoindentation with an $R_{tip} \approx 2.5$ μm spherical tip showed moduli in the range of 36 ± 7 kPa (reported as mean ± SD, outer zone) to 60 ± 15 kPa (inner zone) (Sanchez-Adams et al., 2013). For human meniscus surface, instrumented microindentation with an $R_{tip} \approx 150$ μm spherical tip showed steady state modulus of 1.65 ± 0.13 MPa for 57 – 70 years old tissues (Moyer et al., 2012). This markedly higher E_{ind} of murine meniscus is likely associated with their smaller body weight than other species. Recently, a negative allometric scaling was found between articular cartilage thickness and body mass across many species, including mouse, human and others. This relation was hypothesized to contribute to a decrease in cartilage biomechanical properties as increasing body weight (Malda et al., 2013). This hypothesis was supported by our previous nanoindentation work on wild-type murine knee cartilage, where murine cartilage was found to be significantly stiffer (E_{ind} ~ 1 MPa) (Batista et al., 2014) than cartilage of larger species, including porcine (McLeod et al., 2013), bovine (Nia et al., 2011) and human (Stolz et al., 2009) tissues (E_{ind} ~ 0.1 MPa). For meniscus, there has been no systematic study on the relationship between body mass and tissue size across species. However, since the thickness of meniscus is similar to articular cartilage in both mouse (~ 50 – 100 μm in the central region, Fig. 1a) and human (~ 2 mm (Wenger et al., 2013)), it is likely that similar allometric scaling law is also

present. As supported by recent tissue-level studies of meniscus (Joshi et al., 1995; Sweigart et al., 2004), macroindentation measurements found that the smaller lapine menisci had significantly higher aggregate moduli than the larger human, porcine and bovine tissues (Sweigart et al., 2004).

4.5 Comparison to murine articular cartilage

The moduli of murine meniscus surface were significantly higher than its direct contact counterpart, the articular cartilage (E_{ind} = 1.4 ± 0.1 MPa, Fig. 5b). In addition, as shown in this and previous (Batista et al., 2014) studies, indentation of articular cartilage resulted in typical Hertzian-like *F-D* curves (Fig. 5a). The surface layer of articular cartilage is mostly composed of transversely aligned, type II-dominated collagen fibrils, with higher proteoglycan concentrations than meniscus (Xia et al., 2008). The lower cartilage moduli are likely associated with the less organized, less densely packed, or less pre-stretched collagen fibril networks on the surface. In comparison to meniscus, the presence of abundant proteoglycans in articular cartilage may also contribute to the stress localization and higher degree of isotropy, and thus, lead to more Hertzian-like indentation behaviors.

4.6 Implications for murine model-based osteoarthritis studies

Mechanical knowledge obtained in this study can be applied to murine-based osteoarthritis studies. Recently, AFM-based nanomechanical tests on murine cartilage have become a valuable tool for investigating the articular cartilage biomechanical function and pathogenesis of OA (Batista et al., 2014; Nia et al., 2015; Stolz et al., 2009; Willard et al., 2014). The successful execution of AFM-based nanoindentation on murine cartilage demonstrated the potential of using similar approaches to provide valuable insights into the roles of meniscus in the development of OA. While OA is now recognized as a whole-joint disease (Poole, 2012), understanding of the function of meniscus and its interaction with articular cartilage during OA progression is very limited. A biomechanical focus on murine meniscus can thus provide a novel platform for investigating individual mechanical changes of joint tissues that occur and result in OA. For example, it is suggested that in articular cartilage, OA initiates from superficial layer before propagating to the interior (Saarakkala et al., 2010), while the propagation pattern for OA in meniscus is unclear (Pauli et al., 2011). Based on the knowledge of healthy, normal mice, future studies on the concomitant mechanical changes at the meniscus-cartilage contact interfaces may be used as a novel biomarker for the detection and evaluation of OA when combined with clinically relevant OA models, such as the destabilization of the medial meniscus surgery (Glasson et al., 2007).

5. Conclusions

In this study, we quantified the nanomechanical properties of murine meniscus surface via AFM-based nanoindentation. A non-Hertzian, linear *F-D* indentation response was detected on normal, healthy murine meniscus surface at 6 – 24 weeks age. This behavior is likely associated with the highly anisotropic, circumferential collagen fibril bundle-dominated architecture. The indentation modulus/stiffness showed negligible dependence on tested anatomical locations or mouse age. In addition, murine menisci were found to be ≈ 4 ×

stiffer than murine articular cartilage. To our knowledge, this is the first study that focused on the mechanical properties of murine meniscus. It is hoped that the knowledge obtained here can lay the ground for future explorations of meniscus developmental biology and OA pathology using transgenic or surgery-induced OA models.

Acknowledgments

This work was supported by the Faculty Start-up Grant at Drexel University (LH), the National Institutes of Health (grants AR063905 to VR and AR033236 to CO and AJG). We also thank Dr. R. L. Mauck, Dr. L. J. Soslowsky and Dr. V. B. Shenoy for valuable discussions.

References

Ameye LG, Young MF. Animal models of osteoarthritis: lessons learned while seeking the 'Holy Grail'. Curr. Opin. Rheumatol. 2006; 18:537–547. [PubMed: 16896297]

Andriacchi TP, Mundermann A, Smith RL, Alexander EJ, Dyrby CO, Koo S. A framework for the in vivo pathomechanics of osteoarthritis at the knee. Ann. Biomed. Eng. 2004; 32:447–457. [PubMed: 15095819]

Aspden RM, Yarker YE, Hukins DWL. Collagen orientations in the meniscus of the knee joint. J. Anat. 1985; 140:371–380. [PubMed: 4066476]

Baro VJ, Bonnevie ED, Lai X, Price C, Burris DL, Wang L. Functional characterization of normal and degraded bovine meniscus: rate-dependent indentation and friction studies. Bone. 2012; 51:232–240. [PubMed: 22449445]

Batista MA, Nia HT, Önnerfjord P, Cox KA, Ortiz C, Grodzinsky AJ, Heinegård D, Han L. Nanomechanical phenotype of chondroadherin-null murine articular cartilage. Matrix Biol. 2014; 38:84–90. [PubMed: 24892719]

Bray DF, Bagu J, Koegler P. Comparison of hexamethyldisilazane (HMDS), peldri II, and critical-point drying methods for scanning electron-microscopy of biological specimens. Microsc. Res. Tech. 1993; 26:489–495. [PubMed: 8305726]

Englund M. The role of the meniscus in osteoarthritis genesis. Rheum. Dis. Clin. North Am. 2008; 34:573–579. [PubMed: 18687273]

Fang H, Beier F. Mouse models of osteoarthritis: modelling risk factors and assessing outcomes. Nat. Rev. Rheumatol. 2014; 10:413–421. [PubMed: 24662645]

Fithian DC, Kelly MA, Mow VC. Material properties and structure-function-relationships in the menisci. Clin. Orthop. Relat. Res. 1990; 252:19–31. [PubMed: 2406069]

Glasson SS, Blanchet TJ, Morris EA. The surgical destabilization of the medial meniscus (DMM) model of osteoarthritis in the 129/SvEv mouse. Osteoarthr. Cartilage. 2007; 15:1061–1069.

Han L, Frank EH, Greene JJ, Lee H-Y, Hung H-HK, Grodzinsky AJ, Ortiz C. Time-dependent nanomechanics of cartilage. Biophys. J. 2011; 100:1846–1854. [PubMed: 21463599]

Herwig J, Egner E, Buddecke E. Chemical changes of human knee joint menisci in various stages of degeneration. Ann. Rheum. Dis. 1984; 43:635–640. [PubMed: 6548109]

Hunter DJ, Zhang YQ, Niu JB, Tu X, Amin S, Clancy M, Guermazi A, Grigorian M, Gale D, Felson DT. The association of meniscal pathologic changes with cartilage loss in symptomatic knee ostoearthritis. Arthritis Rheum. 2006; 54:795–801. [PubMed: 16508930]

Joshi MD, Suh JK, Marui T, Woo SLY. Interspecies variation of compressive biomechanical properties of the meniscus. J. Biomed. Mater. Res. 1995; 29:823–828. [PubMed: 7593020]

Katsuragawa Y, Saitoh K, Tanaka N, Wake M, Ikeda Y, Furukawa H, Tohma S, Sawabe M, Ishiyama M, Yagishita S, Suzuki R, Mitomi H, Fukui N. Changes of human menisci in osteoarthritic knee joints. Osteoarthr. Cartilage. 2010; 18:1133–1143.

Klompmaker J, Jansen HW, Veth RP, Nielsen HK, de Groot JH, Pennings AJ, Kuijer R. Meniscal repair by fibrocartilage? An experimental study in the dog. J. Orthop. Res. 1992; 10:359–370. [PubMed: 1569499]

Lai JH, Levenston ME. Meniscus and cartilage exhibit distinct intra-tissue strain distributions under unconfined compression. Osteoarthr. Cartilage. 2010; 18:1291–1299.

Makris EA, Hadidi P, Athanasiou KA. The knee meniscus: structure-function, pathophysiology, current repair techniques, and prospects for regeneration. Biomaterials. 2011; 32:7411–7431. [PubMed: 21764438]

Malda J, de Grauw JC, Benders KEM, Kik MJL, van de Lest CHA, Creemers LB, Dhert WJA, van Weeren PR. Of mice, men and elephants: the relation between articular cartilage thickness and body mass. PLoS One. 2013; 8:e57683. [PubMed: 23437402]

Maroudas A, Bayliss MT, Uchitel-Kaushansky N, Schneiderman R, Gilav E. Aggrecan turnover in human articular cartilage: use of aspartic acid racemization as a marker of molecular age. Arch. Biochem. Biophys. 1998; 350:61–71. [PubMed: 9466821]

McLeod MA, Wilusz RE, Guilak F. Depth-dependent anisotropy of the micromechanical properties of the extracellular and pericellular matrices of articular cartilage evaluated via atomic force microscopy. J. Biomech. 2013; 46:586–592. [PubMed: 23062866]

Moyer JT, Abraham AC, Donahue TLH. Nanoindentation of human meniscal surfaces. J. Biomech. 2012; 45:2230–2235. [PubMed: 22789734]

Moyer JT, Priest R, Bouman T, Abraham AC, Donahue TLH. Indentation properties and glycosaminoglycan content of human menisci in the deep zone. Acta Biomater. 2013; 9:6624–6629. [PubMed: 23321302]

Nia HT, Gauci S, Azadi M, Hung H-H, Frank E, Fosang A, Ortiz C, Grodzinsky AJ. High-bandwidth AFM-based rheology is a sensitive indicator of early cartilage aggrecan degradation relevant to mouse models of osteoarthritis. J. Biomech. 2015; 48:162–165. [PubMed: 25435386]

Nia HT, Han L, Li Y, Ortiz C, Grodzinsky AJ. Poroelasticity of cartilage at the nanoscale. Biophys. J. 2011; 101:2304–2313. [PubMed: 22067171]

Pauli C, Grogan SP, Patil S, Otsuki S, Hasegawa A, Koziol J, Lotz MK, D'Lima DD. Macroscopic and histopathologic analysis of human knee menisci in aging and osteoarthritis. Osteoarthr. Cartilage. 2011; 19:1132–1141.

Pedersen HE. The ossicles of the semilunar cartilages of rodents. Anat. Rec. 1949; 105:1–9. [PubMed: 15393663]

Petersen W, Tillmann B. Collagenous fibril texture of the human knee joint menisci. Anat. Embryol. 1998; 197:317–324. [PubMed: 9565324]

Poole AR. Osteoarthritis as a whole joint disease. HSSJ. 2012; 8:4–6.

Proctor CS, Schmidt MB, Whipple RR, Kelly MA, Mow VC. Material properties of the normal medial bovine meniscus. J. Orthop. Res. 1989; 7:771–782. [PubMed: 2677284]

Rojas FP, Batista MA, Lindburg CA, Dean D, Grodzinsky AJ, Ortiz C, Han L. Molecular adhesion between cartilage extracellular matrix macromolecules. Biomacromolecules. 2014; 15:772–780. [PubMed: 24491174]

Saarakkala S, Julkunen P, Kiviranta P, Makitalo J, Jurvelin JS, Korhonen RK. Depth-wise progression of osteoarthritis in human articular cartilage: investigation of composition, structure and biomechanics. Osteoarthr. Cartilage. 2010; 18:73–81.

Sakai M. Time-dependent viscoelastic relation between load and penetration for an axisymmetric indenter. Philos. Mag. A. 2002; 82:1841–1849.

Sanchez-Adams J, Wilusz RE, Guilak F. Atomic force microscopy reveals regional variations in the micromechanical properties of the pericellular and extracellular matrices of the meniscus. J. Orthop. Res. 2013; 31:1218–1225. [PubMed: 23568545]

Skaggs DL, Warden WH, Mow VC. Radial tie fibers influence the tensile properties of the bovine medial meniscus. J. Orthop. Res. 1994; 12:176–185. [PubMed: 8164089]

Somerville JM, Aspden RM, Armour KE, Armour KJ, Reid DM. Growth of C57BL/6 mice and the material and mechanical properties of cortical bone from the tibia. Calcif. Tissue Int. 2004; 74:469–475. [PubMed: 14961209]

Soulhat J, Buschmann MD, Shirazi-Adl A. A fibril network reinforced biphasic model of cartilage in uniaxial compression. J. Biomech. Eng. 1999; 121:340–347. [PubMed: 10396701]

Spilker RL, Donzelli PS, Mow VC. A transversely isotropic biphasic finite element model of the meniscus. J. Biomech. 1992; 25:1027–1045. [PubMed: 1517263]

Stolz M, Gottardi R, Raiteri R, Miot S, Martin I, Imer R, Staufer U, Raducanu A, Düggelin M, Baschong W, Daniels AU, Friederich NF, Aszodi A, Aebi U. Early detection of aging cartilage and osteoarthritis in mice and patient samples using atomic force microscopy. Nat. Nanotechnol. 2009; 4:186–192. [PubMed: 19265849]

Sweigart MA, Athanasiou KA. Tensile and compressive properties of the medial rabbit meniscus. Proc. Inst. Mech. Eng. [H]. 2005; 219:337–347.

Sweigart MA, Zhu CF, Burt DM, deHoll PD, Agrawal CM, Clanton TO, Athanasiou KA. Intraspecies and interspecies comparison of the compressive properties of the medial meniscus. Ann. Biomed. Eng. 2004; 32:1569–1579. [PubMed: 15636116]

Vanden Berg-Foels WS, Scipioni L, Huynh C, Wen X. Helium ion microscopy for high-resolution visualization of the articular cartilage collagen network. J. Microsc. 2012; 246:168–176. [PubMed: 22416783]

Verzijl N, DeGroot J, Thorpe SR, Bank RA, Shaw JN, Lyons TJ, Bijlsma JWJ, Lafeber FPJG, Baynes JW, TeKoppele JM. Effect of collagen turnover on the accumulation of advanced glycation end products. J. Biol. Chem. 2000; 275:39027–39031. [PubMed: 10976109]

Voloshin AS, Wosk J. Shock absorption of meniscectomized and painful knees: a comparative in vivo study. J. Biomed. Eng. 1983; 5:157–161. [PubMed: 6687914]

Walker PS, Erkman MJ. The role of the menisci in force transmission across the knee. Clin. Orthop. Relat. Res. 1975:184–192. [PubMed: 1173360]

Wang H, Abhilash AS, Chen CS, Wells RG, Shenoy VB. Long range force transmission in fibrous matrices enabled by tension-driven alignment of fibers. Biophys. J. 2014; 107:2592–2603. [PubMed: 25468338]

Wenger A, Wirth W, Hudelmaier M, Noebauer-Huhmann I, Trattnig S, Bloecker K, Frobell RB, Kwoh CK, Eckstein F, Englund M. Meniscus body position, size, and shape in persons with and persons without radiographic knee osteoarthritis: quantitative analyses of knee magnetic resonance images from the osteoarthritis initiative. Arthritis Rheum. 2013; 65:1804–1811. [PubMed: 23529645]

Willard VP, Diekman BO, Sanchez-Adams J, Christoforou N, Leong KW, Guilak F. Use of cartilage derived from murine induced pluripotent stem cells for osteoarthritis drug screening. Arthritis Rheum. 2014; 66:3062–3072.

Xia Y, Zheng S, Bidthanapally A. Depth-dependent profiles of glycosaminoglycans in articular cartilage by μMRI and histochemistry. J. Magn. Reson. Imaging. 2008; 28:151–157. [PubMed: 18581328]

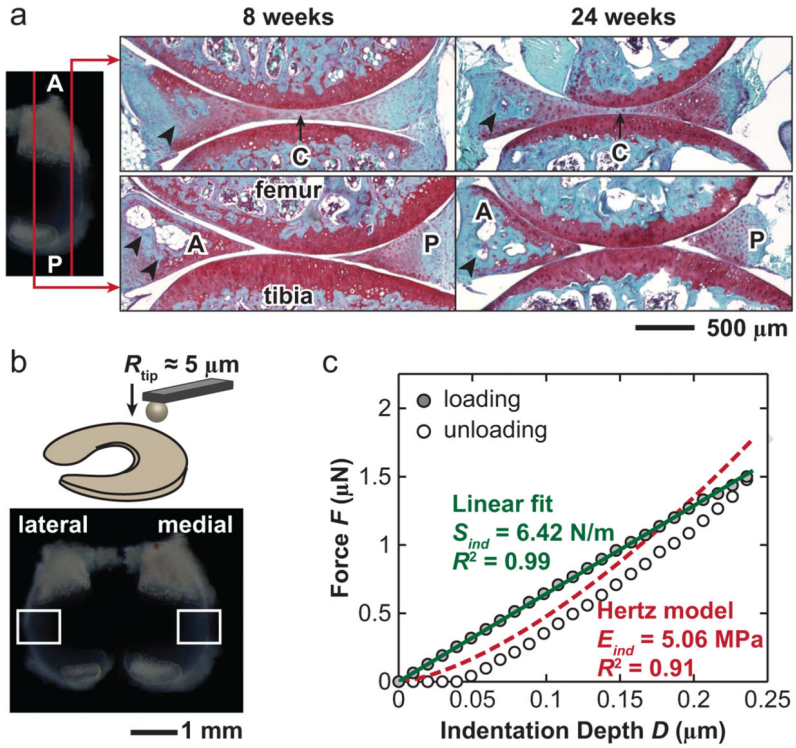

Fig. 1.

Nanoindentation of murine meniscus surface. (a) Safranin-O/FastGreen histological staining of the sagittal cross-section of the medial compartments from 8- and 24-week old murine knees. Increased ossification at the anterior (A) and posterior (P) horns with age was shown as white-to-blue staining (black arrowheads). The ~ 50 – 100 μm thick central region (C) for nanoindentation test was not ossified. (b) Schematic of AFM-based nanoindentation on murine meniscus, where the two squares highlight the regions of interest, i.e., the proximal side, central region of each meniscus surface. (c) Typical indentation force versus depth (*F-D*) curve on one 8-week old murine medial meniscus at 10 μm/s indentation depth rate. The linear fit on the loading curve yields higher coefficient of determination, R^2, than the Hertz model.

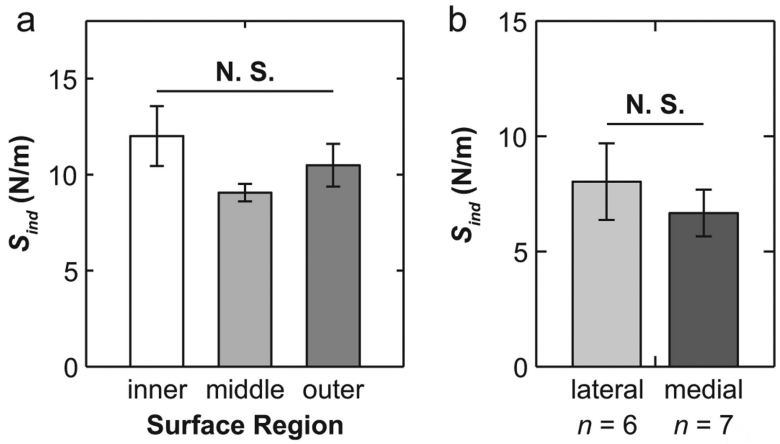

Fig. 2.

Absence of mechanical heterogeneity across different anatomical sites. (a) Effective indentation stiffness, S_{ind}, showed no significant difference within the inner, middle and outer surface regions, measured on the meniscus central region of one 6-week old mouse (mean ± SEM of Ł 8 locations in each region, $p > 0.05$ via Kruskal-Wallis test). (b) S_{ind} of lateral versus medial menisci showed no significant difference (mean ± SEM of the average S_{ind} measured on each 12-week old meniscus, $n = 6$ for lateral and $n = 7$ for medial menisci, $p > 0.05$ via Mann-Whitney U test). All the values were measured at 10 μm/s indentation depth rate.

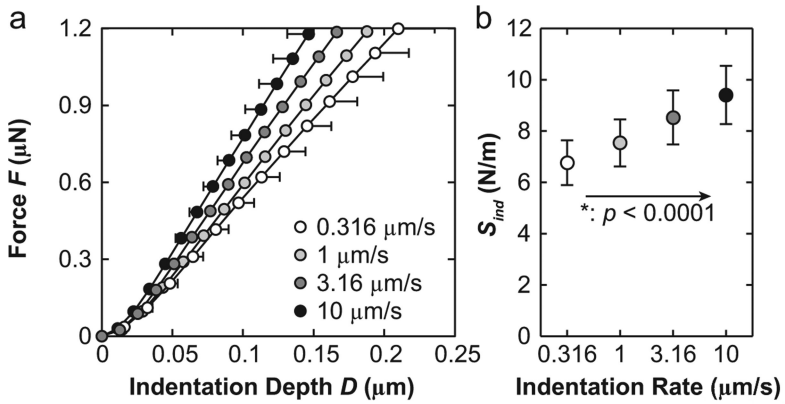

Fig. 3.

Indentation rate-dependent mechanical properties of murine meniscus surface. (a) Indentation force versus depth curves at 0.316 – 10 μm/s indentation depth rates. (b) Significant rate dependence of S_{ind} was detected via Friedman's test ($p < 0.0001$). For both panels, data shown are mean ± SEM of Ł 8 locations on one 8-week old medial meniscus.

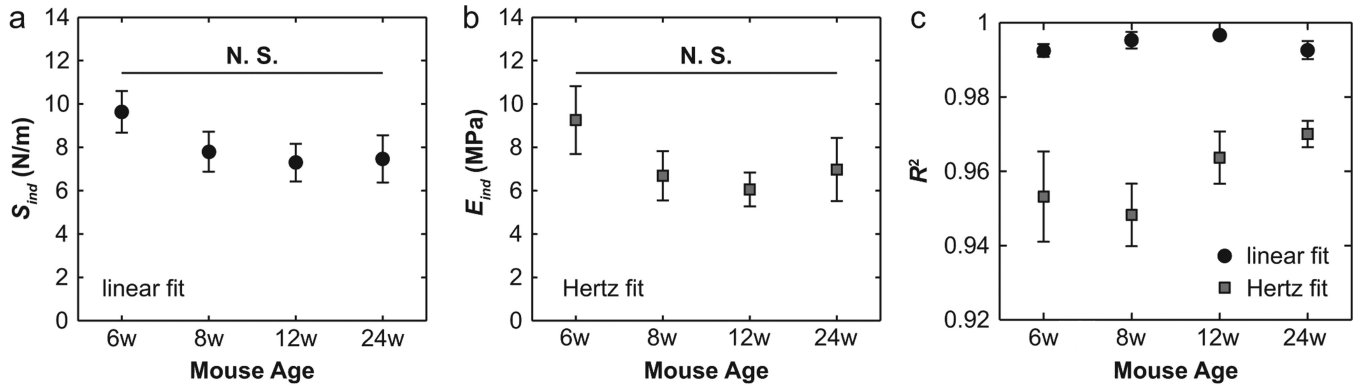

Fig. 4.

Mechanical properties of murine meniscus surface at different ages. (a, b) Effective indentation stiffness, S_{ind} (a), and modulus, E_{ind} (b), of proximal side meniscus surface at 6 weeks (n = 5), 8 weeks (n = 10), 12 weeks (n = 13) and 24 weeks (n = 5) of ages showed no significant age dependence ($p > 0.05$ via Kruskal-Wallis test). (c) Comparison of coefficient of determination, R^2, calculated via the fits of S_{ind} and E_{ind}, respectively. The linear fit yields significantly higher R^2 than the Hertz model ($p < 0.0001$ via Wilcoxon signed rank test). For all three panels, data shown are mean ± SEM of the average values measured on meniscus at the given age cohort at 10 μm/s indentation depth rate.

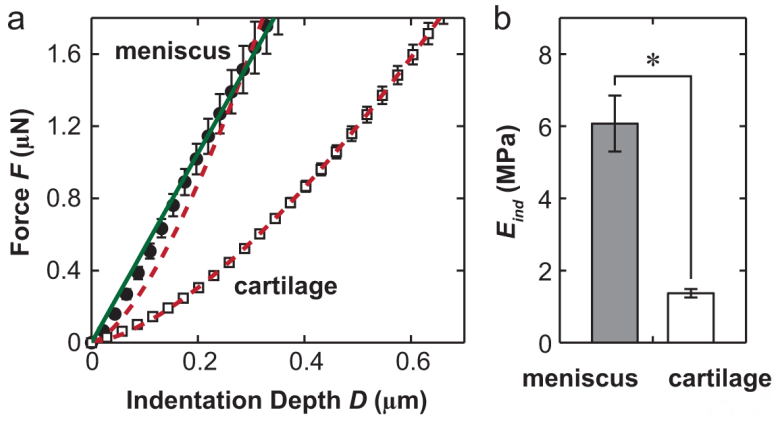

Fig. 5.

Comparison of the mechanical properties between murine meniscus and cartilage surfaces. (a) Typical indentation *F-D* curves on the one medial meniscus and medial condyle cartilage (mean ± SEM of Ł 10 positions each, 12 weeks age). The green solid line is the linear fit for meniscus data, and red dashed lines are Hertzian fits for both. (b) Meniscus surfaces (n = 13) showed significantly higher E_{ind} than articular cartilage surfaces (n = 6) at 12 weeks age (*: $p < 0.0001$ via Mann-Whitney U test). All the data were measured at 10 μm/s indentation depth rate.

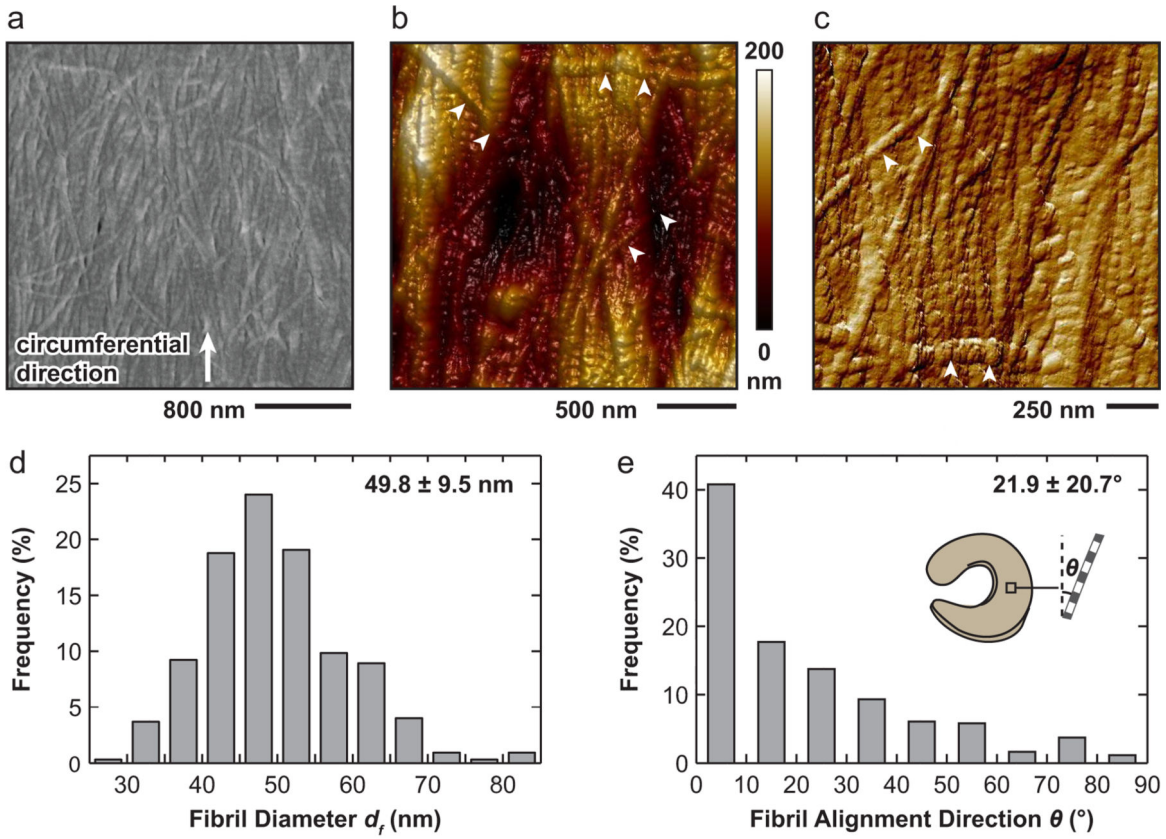

Fig. 6.

Collagen architecture of murine meniscus surface. Typical (a) SEM and tapping mode AFM (b) height and (c) amplitude images at different scales show that collagen fibrils are mostly aligned as bundles along the circumferential direction on meniscus surface, interdigitated by transversely aligned fibrils (white arrowheads in b). (d, e) Histograms of (d) collagen diameter and (e) collagen alignment with respect to the circumferential direction, respectively. Values reported are mean ± STD of 325 fibrils for diameter (232 from SEM, 93 from AFM), and 429 fibrils for alignment direction (324 from SEM, 105 from AFM) from six 12-week old medial menisci.